PHYSICAL REVIEW D **88,** 076006 (2013)

Spectral method for the Cornell and screened Cornell potentials in momentum space

Jiao-Kai Chen*

School of Physics and Information Science, Shanxi Normal University, Linfen 041004, China

(Received 15 September 2013; published 10 October 2013)

We employ the Landé subtraction method and the spectral method to solve numerically the Schrödinger equation in momentum space with the Cornell and screened Cornell potentials in a unified approach. The calculated results are excellent, because singularities, especially the double-pole singularity, possessed by potentials are handled completely. Besides, we notice that the eigenvalues yielded by numerical methods have definite convergence directions. The convergence directions of the calculated eigenvalues are abnormal when potentials are singular and become normal as singularities are manipulated properly.

DOI: 10.1103/PhysRevD.88.076006 PACS numbers: 11.10.St, 02.60.Nm, 03.65.Ge, 12.39.Pn

I. INTRODUCTION

Heavy quarkonium spectroscopy [1–5] is a keystone experimental output. The spectrum of states can be well described by using a simple potential model. One of the well-known potentials [6–13] is the so-called Cornell potential [6,7],

$$V(r) = -\frac{\alpha}{r} + \lambda r, \tag{1}$$

where the first term denotes the color Coulomb potential for short distances, and the second term denotes the linear potential for long distances, which has been validated by lattice QCD calculations. Indeed, the vacuum polarization induced by the dynamical quark pair creation will soften the linear potential and cause the screening effect [14–16]. In this paper, the considered screened Cornell potential takes the form [17–25]

$$V_{\mathrm{SC}}(r) = -\frac{\alpha}{r}e^{-\beta r} + \frac{\lambda}{\eta}(1 - e^{-\eta r}), \tag{2}$$

where β and η are the screening parameters for the screened Coulomb potential and the screened linear potential, respectively. As $\beta,\ \eta \to 0$, the screened Cornell potential approaches the Cornell potential; hence, the Cornell potential is regarded as a special case of the screened Cornell potential in this paper.

The Cornell and screened Cornell potentials can be handled very easily in configuration space. But when considering the relativistic effects and retardation effects [26], doing calculations in momentum space will be much more economic. The major difficulty in solving the momentum-space integral equation with the screened Cornell potential is the double-pole singularity [27] possessed by potential. In Refs. [28,29], singularity was handled by introducing an arbitrary cutoff in potential. In contrast to the difficulty for the expansion method [30–32] or for the variational method [33–36], the difficulty for the quadrature method [17,37–41] will be much more severe. In Ref. [32], by implementing the Landé subtraction method [17,26,32,37,42–44], the double-pole singularity was weakened and a principal-value singularity is left, and then the remaining singularity was tackled by expanding the wave function in a suitable set of basis functions and employing the method presented in Ref. [45]. In Ref. [37], the author firstly weakened the double-pole singularity by the Landé subtraction method just as in Ref. [32], then applied the Nyström-plus-correction method to solve the integral equation with the principal-value singularity. We discussed the screened Cornell potential problem [17] by employing the Landé subtraction method and the Nyström method, but the accuracy of results cannot reach very high, as the screening parameters are small because of the left Cauchy principal-value singularity. In Ref. [46], a spectral method was proposed to handle the double-pole singularity possessed by the momentum-space Cornell potential, but this method is not easily generalizable for the screened Cornell potential, and cannot handle the Cornell and screened Cornell potentials in a unified approach due to the term λ/η; see Eq. (2).

In this paper, we will present a combined method which is applicable for both the Cornell and screened Cornell potentials, and also applicable for the linear and screened linear potentials. We firstly apply the Landé subtraction method to remove the logarithmic singularity and to relieve the double-pole singularity to be a principal-value singularity, and then handle the remaining principal-value singularity, which is absorbed into the quadrature weights. As expected, the calculated eigenvalues are very good when singularities are handled completely. Besides, we notice that the convergence directions (see the Appendix for more details) of the obtained eigenvalues when the singularities are completely handled are different from those when the potentials are singular. In Refs. [17,47], the furcation phenomenon [48] was proposed as an indicator for the bad behavior of the bad solutions and the bad behavior of the integrands (or kernels). The abnormal convergence direction phenomenon observed in this paper is expected to play a similar role to the furcation phenomenon. One of the differences between them is that the furcation phenomenon

*chenjk@sxnu.edu.cn

emerges in the calculated eigenfunctions, while the convergence direction is about the eigenvalues.

This paper is organized as follows: In Sec. II, the double-pole singularity is handled analytically by employing the Landé subtraction method. In Sec. III, the spectral method is applied to tackle the principal-value singularity. The obtained numerical results are presented in Sec. IV. Finally, we conclude in Sec. V.

II. ANALYTICAL TREATMENT

In this section, we first represent the screened Cornell potential in momentum space. Then, we employ the Landé subtraction method to weaken or eliminate singularities in potential.

A. Screened Cornell potential in momentum space

By the Fourier transform

$$V(\mathbf{q}) = \int V'(\mathbf{r}) e^{-i\mathbf{q}\cdot\mathbf{r}} d\mathbf{r}, \qquad V'(\mathbf{r}) = (2\pi)^{-3} \int V(\mathbf{q}) e^{i\mathbf{q}\cdot\mathbf{r}} d\mathbf{q}, \tag{3}$$

the screened Cornell potential [Eq. (2)] is written in momentum space as

$$V_{\mathrm{SC}}(\mathbf{q}) = -\frac{4\pi\alpha}{\beta^2+\mathbf{q}^2} + (2\pi)^3 \frac{\lambda}{\eta}\left[\delta(\mathbf{q}) + \frac{1}{2\pi^2}\frac{\partial}{\partial\eta}\left(\frac{1}{\eta^2+\mathbf{q}^2}\right)\right]. \tag{4}$$

Then, applying the formula

$$V^l(p,p') = \int d\Omega Y_{lm}(\Omega) \int d\Omega' Y_{l'm'}(\Omega') V(\mathbf{q}), \tag{5}$$

the screened Cornell potential [Eq. (4)] is expanded in partial waves as [17]

$$V^l_{\mathrm{SC}}(p,p') = -8\pi^2\alpha \frac{Q_l(z_\beta)}{pp'} + (2\pi)^3 \left[\frac{\lambda}{\eta}\frac{\delta(p-p')}{p^2}\delta_{ll'} + \frac{\lambda}{\pi}\frac{Q'_l(z_\eta)}{(pp')^2}\right], \tag{6}$$

where l is the orbital quantum number, z_β and z_η are defined as

$$z_\beta = \frac{p^2+p'^2+\beta^2}{2p'p}, \qquad z_\eta = \frac{p^2+p'^2+\eta^2}{2p'p}, \tag{7}$$

$Q_l(z)$ is the Legendre polynomial of the second kind, and $Q'_l(z)$ is the first derivative of $Q_l(z)$ with respect to z.

From Eq. (6) and the relations

$$Q_l(z) = P_l(z)Q_0(z) - \omega_{l-1}(z), \qquad Q_0(z) = \frac{1}{2}\ln\frac{z+1}{z-1}, \qquad \omega_{l-1}(z) = \sum_{m=1}^{l}\frac{1}{m}P_{l-m}(z)P_{m-1}(z), \tag{8}$$

and

$$Q'_l(z) = P'_l(z)Q_0(z) + P_l(z)Q'_0(z) - w'_{l-1}(z), \tag{9}$$

it is obvious that the singularities of $V^l_{\mathrm{SC}}(p,p')$ come from $Q_0(z)$ and $Q'_0(z)$. $Q_0(z)$ has a logarithmic singularity as $z \to 1$, and $Q'_0(z_\eta)$ has a double-pole singularity at $p = p'$ as $\eta \to 0$. The first term in the second line in Eq. (6) is singular as $\eta \to 0$ and can be canceled out by a new term arising from the Landé subtraction method; see the terms in the parentheses in the first line in Eq. (13).

B. Landé subtraction method

Many integral equations, such as the Dirac, Klein-Gordon, spinless Salpeter, etc., equations, which are with the screened Cornell potential and represented in momentum space, have the same singularity structure as the momentum-space Schrödinger equation. So, we take the Schrödinger equation with the screened Cornell potential as an example in this paper. The partial wave expansion of the momentum-space Schrödinger equation reads [17]

$$E_{nl}\phi_{nl}(p) = \frac{p^2}{2\mu}\phi_{nl}(p) + \frac{1}{(2\pi)^3}\int p'^2 dp' V^l_{\mathrm{SC}}(p,p')\phi_{nl}(p'), \tag{10}$$

where n is the principal quantum number and $V^l_{\mathrm{SC}}(p,p')$ is as given in Eq. (6). Evidently, when the screening parameters β and η are equal to zero, the integral in Eq. (10) has the logarithmic singularity, which can be treated very easily, and the double-pole singularity, on which we concentrate in this paper. Just as discussed in Refs. [17,47], the Schrödinger equation with the screened Cornell potential is still singular [27] even as $\beta,\ \eta > 0$ and also needs to be handled.

In Eq. (10), there are different kinds of integrals. We, here and hereafter, use $\int$ to refer to any definition of the integral such that

$$\int_a^b \frac{f(x)}{(x-y)^p}dx, \qquad p > 0 \tag{11}$$

exists, such as the usual Riemann integral ($p < 1$), the Cauchy principal-value integral ($p = 1$), and the Hadamard finite-part integral or hypersingular integral ($p = 2$) [49,50].

Using the useful identities [17,47,32,51]

$$I_C(z_\eta) = \int_0^\infty \frac{Q_0(z_\eta)}{p'}dp' = \frac{\pi^2}{2} - \pi\arctan\frac{\eta}{p}, \qquad I_L(z_\eta) = \int_0^\infty Q'_0(z_\eta)dp' = -\frac{\pi p^2}{\eta} \tag{12}$$

and applying the Landé subtraction method to handle singularities, the Schrödinger equation [Eq. (10)] is rewritten as

$$E_{nl}\phi_{nl}(p) = \frac{p^2}{2\mu}\phi_{nl}(p) - \frac{\alpha}{\pi}I_C(z_\beta)P_l(z'_\beta)p\phi_{nl}(p) + \frac{\lambda}{\pi p}I_C(z_\eta)P'_l(z'_\eta)\phi_{nl}(p) + \left(\frac{\lambda}{\eta} + \frac{\lambda}{\pi p^2}P_l(z'_\eta)I_L(z_\eta)\right)\phi_{nl}(p)$$
$$- \frac{\alpha}{\pi p}\int_0^\infty \frac{Q_0(z_\beta)}{p'}[p'^2P_l(z_\beta)\phi_{nl}(p') - p^2P_l(z'_\beta)\phi_{nl}(p)]dp' + \frac{\lambda}{\pi p^2}\int_0^\infty \frac{Q_0(z_\eta)}{p'}[P'_l(z_\eta)p'\phi_{nl}(p')$$
$$- P'_l(z'_\eta)p\phi_{nl}(p)]dp' + \frac{\lambda}{\pi p^2}\int_0^\infty Q'_0(z_\eta)[P_l(z_\eta)\phi_{nl}(p') - P_l(z'_\eta)\phi_{nl}(p)]dp'$$
$$+ \frac{\alpha}{\pi p}\int_0^\infty w_{l-1}(z_\beta)p'\phi_{nl}(p')dp' - \frac{\lambda}{\pi p^2}\int_0^\infty w'_{l-1}(z_\eta)\phi_{nl}(p')dp', \tag{13}$$

where

$$z'_\beta = \frac{2p^2+\beta^2}{2p^2}, \qquad z'_\eta = \frac{2p^2+\eta^2}{2p^2}. \tag{14}$$

As $\eta = 0$, the term λ/η in the parentheses in the first line—i.e., the constant r-independent term in the screened linear potential—is canceled out by $\lambda P_l(z'_\eta)I_L(z_\eta)/(\pi p^2)$ arising from the Landé subtraction method; thus, the terms in the parentheses vanish. Therefore, the first line is regular for both $\beta, \eta > 0$ and $\beta, \eta = 0$. The second line is regular because the logarithmic singularity in $Q_0(z)$ is canceled out. The first integral in the third line has the left principal-value singularity after the second-order singularity in $Q'_0(z_\eta)$ is weakened by the subtraction method. The last two terms in the last line are regular. In summary, only the first integral in the last line needs further treatment now. Obviously, the subtracted Eq. (13) is singular in both the Cornell potential case and the screened Cornell potential case [27]. In Eq. (13), we deal with the Cornell potential and the screened Cornell potential in the same manner. Later, we will also cope in the same manner with the left principal-value singularity possessed by these two potentials.

C. Rational map

To deal with the remaining Cauchy principal-value singularity and to apply a numerical method to the integral equation [Eq. (13)], we map the semi-infinite interval $[0, \infty)$ onto some standard finite interval $[a, b]$, which we take to be $[-1, 1)$. In this paper, we may take the rational transformation

$$p = \xi\frac{1+s}{1-s}, \qquad p' = \xi\frac{1+t}{1-t}, \tag{15}$$

where ξ is a numerical parameter providing additional control of the rate of convergence. Then we have

$$dp' = \frac{2\xi}{(1-t)^2}dt. \tag{16}$$

The subtracted Eq. (13) can be rewritten easily using the variables s and t. We focus on the first integral in the last line in Eq. (13), and rewrite it as a Cauchy principal-value integral in an explicit form:

$$\int_0^\infty Q'_0(z_\eta)[P_l(z_\eta)\phi_{nl}(p') - P_l(z'_\eta)\phi_{nl}(p)]dp'$$
$$= \int_{-1}^1 \frac{F_1(s,t)F_2(s,t)}{s-t}\frac{2\xi}{(1-t)^2}dt, \tag{17}$$

where $F_1(s,t)$ and $F_2(s,t)$ are regular functions,

$$F_1(s,t) = (s-t)^2Q'_0(z_\eta),$$
$$F_2(s,t) = \frac{P_l(z_\eta)\phi_{nl}(p') - P_l(z'_\eta)\phi_{nl}(p)}{s-t}, \tag{18}$$

and p, p', z_η, and z'_η are functions of s and t; see Eqs. (14) and (15). When $t \to s$, $F_1(s,t)$ is finite in the case of the Cornell potential ($\eta = 0$) and is equal to zero in the case of the screened Cornell potential ($\eta > 0$). For both the Cornell and the screened Cornell potentials, $F_2(s,t)$ is the derivative with respect to t at point $t = s$:

$$\lim_{t\to s}F_2(s,t) = -\frac{\partial}{\partial t}[P_l(z_\eta)\phi_{nl}(p')]. \tag{19}$$

III. NUMERICAL METHOD

In this section, we will apply the Gauss-Legendre quadrature rule to the regular integral and the Cauchy principal value integral, which will transform the subtracted integral equation [Eq. (13)] into a matrix equation which is free of singularities. We will also give discussions of the calculated eigenvalues on the mapping parameter ξ.

A. Legendre polynomial

For completeness, we list the formulas which are useful in this paper. The Legendre polynomial [52,53] of degree n is defined by

$$P_n(x) = \frac{1}{2^n n!}\frac{d^n}{dx^n}(x^2-1)^n,$$

and the orthogonality property is

$$\int_{-1}^1 P_m(x)P_n(x)dx = \frac{2}{2n+1}\delta_{nm}. \tag{20}$$

For $z \in (1, \infty)$, the Legendre polynomial of the second kind is defined by

$$Q_n(z) = \frac{1}{2}\int_{-1}^{1}\frac{P_n(x)}{z-x}dx, \tag{21}$$

and there are the relations in Eq. (8). When $z \in (-1, 1)$, $Q_n(z)$ is defined as

$$\begin{aligned} Q_n(z) &= \frac{1}{2}[Q_n(z+i0) + Q_n(z-i0)] \\ &= P_n(z)Q_0(z) - w_{n-1}(z), \end{aligned} \tag{22}$$

where

$$Q_0(z) = \frac{1}{2}\ln\frac{1+z}{1-z}. \tag{23}$$

Except for the expression of $Q_0(z)$, the forms of the formulas in Eqs. (8) and (21) hold for $|z| < 1$.

B. Gauss-Legendre quadrature

One continuous and bounded function can be approximated in the $(-1, 1)$ interval by the Legendre polynomials,

$$f(x) \approx f_N(x) = \sum_{n=0}^{N} a_n P_n(x), \tag{24}$$

where the coefficients a_n are given by

$$\begin{aligned} a_n &= \frac{2n+1}{2}\int_{-1}^{1} f(x)P_n(x)dx \\ &\approx \frac{2n+1}{2}\sum_{i=0}^{N} w_i f(x_i)P_n(x_i). \end{aligned} \tag{25}$$

In the above equation, the quadrature points x_i are the zeros of the Legendre polynomial $P_{N+1}(x)$, and the weights read

$$w_i = \frac{2}{(1-x_i^2)[P'_{N+1}(x_i)]^2}, \tag{26}$$

where the prime stands for the derivative. Substituting Eq. (25) into Eq. (24) gives

$$\begin{aligned} f(x) &\approx f_N(x) = \sum_{i=0}^{N} W_i(x)f(x_i), \\ W_i(x) &= w_i\sum_{n=0}^{N}\frac{2n+1}{2}P_n(x_i)P_n(x). \end{aligned} \tag{27}$$

Equation (27) can be also expressed in another form as

$$f(x) \approx f_N(x) = \sum_{i=0}^{N}\frac{P_{N+1}(x)}{(x-x_i)P'_{N+1}(x_i)}f(x_i), \tag{28}$$

and the remainder $R_N(x)$ is

$$\begin{aligned} R_N(x) &= f(x) - f_N(x) = \frac{f^{(N+1)}(\zeta)}{(N+1)!}\varpi_{N+1}(x), \\ \varpi_{N+1}(x) &= \prod_{i=0}^{N}(x-x_i). \end{aligned} \tag{29}$$

The remainder will become very small if N is large enough.

Using Eq. (20), the Gauss-Legendre quadrature formula for regular integral reads from Eq. (27)

$$\int_{-1}^{1} f(x)dx \approx \sum_{i=0}^{N} w_i f(x_i). \tag{30}$$

Using Eqs. (21) and (27), the principal-value integration can be performed [54,55]:

$$\begin{aligned} \int_{-1}^{1}\frac{f(x)}{y-x}dx &\approx \sum_{i=0}^{N}\tilde{w}_i f(x_i), \\ \tilde{w}_i(y) &= w_i\sum_{n=0}^{N}(2n+1)P_n(x_i)Q_n(y). \end{aligned} \tag{31}$$

By differentiating Eq. (27), we obtain the derivative of the function $f'_N(x)$,

$$\begin{aligned} f'_N(x) &= \sum_{i=0}^{N} W'_i(x)f(x_i), \\ W'_i(x) &= w_i\sum_{n=0}^{N}\frac{2n+1}{2}P_n(x_i)P'_n(x), \end{aligned} \tag{32}$$

where w_i is as in Eq. (26).

C. Effects of parameter ξ

All parameters occurring in this paper can be categorized into two classes. One class includes the physical parameters which are related with the discussed problems, such as the reduced mass μ, the strong coupling constant α, the string tension λ, and the screening factors β and η. The other class includes the numerical parameters which are introduced by the numerical method and are related to the accuracy of the calculated results, such as the number of points of Gaussian quadrature N, and the mapping parameter ξ. Obviously, the accuracy will increase as N increases. ξ also has an effect on the accuracy by changing the distribution of the nodes of the wave functions in the interval $(-1, 1)$.

For simplicity, we write the partial-wave Schrödinger equation in momentum space as

$$E\phi(p) = \int_0^\infty K(p, p')\phi(p')p'^2dp', \tag{33}$$

where

$$K(p, p') = \frac{1}{2\mu}\delta(p-p') + \frac{1}{(2\pi)^3}V^l_{\mathrm{SL}}(p, p'). \tag{34}$$

Defining a functional F in inner-product notation [38,39],

$$F(\psi) = \frac{(\psi, K\psi)}{(\psi, \psi)}, \tag{35}$$

which is usually referred to as the Rayleigh quotient. Expanding the function

$$\psi(p) = \sum_i c_i \phi_i(p), \tag{36}$$

assuming the exact eigenvalues belonging to the kernel K are monotonic and have the same sign,

$$E_{\min} < E_1 < \cdots < E_n < \cdots < E_{\max}. \tag{37}$$

Then, by applying the expansion theorem [56] for the eigenvalue integral equation,

$$K(p, p') = \sum_i E_i \phi_i(p) \phi_i^\dagger(p'), \tag{38}$$

we can obtain

$$E_{\min} \le F(\psi), \qquad F(\psi) \le E_{\max}. \tag{39}$$

The analytical conclusion holds for the numerical results if the chosen numerical methods are good and give small errors.

By using the variables s and t defined in Eq. (15), Eq. (33) can be rewritten in the following form:

$$E\hat{\phi}(s) = \int_{-1}^{1} \hat{K}(s, t)\hat{\phi}(t)\left(\xi\frac{1+t}{1-t}\right)^2 \frac{2\xi}{(1-t)^2}\, dt, \tag{40}$$

where

$$\hat{\phi}(s) = \phi(p), \quad \hat{K}(s,t) = K(p,p'), \quad \hat{\phi}(t) = \phi(p'). \tag{41}$$

Evidently, the exact solutions, the eigenvalues E and the corresponding eigenfunctions $\hat{\phi}(s)$, are independent of ξ.

Employing the Gaussian quadrature rule, the integral in Eq. (40) is transformed into a matrix equation,

$$E\hat{\phi}(s_i) = \sum_{j=0}^{N} w_j \hat{K}(s_i, t_j)\hat{\phi}(t_j)\left(\xi\frac{1+t_j}{1-t_j}\right)^2 \frac{2\xi}{(1-t_j)^2} + R(s, t, \xi), \tag{42}$$

where $R(s, t, \xi)$ is the remainder and is assumed to be small. Neglecting the remainder $R(s, t, \xi)$ and then solving the matrix equation [Eq. (42)], the approximated solutions E and $\hat{\phi}(s)$ are calculated. It is obvious that the obtained solutions are dependent on the parameter ξ. When the chosen Gaussian quadrature rule is appropriate and N is large, the dependence of the solutions on the parameter ξ will be weak. We can see from Eqs. (35) and (39) that the calculated eigenvalues of the matrix equation [Eq. (42)] for the ground state or a lower excited state will be greater than the exact eigenvalues of Eq. (40). The numerical results presented in Sec. IV are consistent with this conclusion.

In practice, the effects of the parameter ξ on the eigenvalues are not as simple as they look. From Eq. (15), we learn that the interval $(0, \xi)$ of the variable p (or q) will be mapped onto the interval $(-1, 0)$ of the variable s (or t), and the interval (ξ, ∞) is mapped onto $(0, 1)$—that is to say, ξ can change the range mapped onto the interval $(-1, 0)$. Besides, the nodes of the wave functions in momentum space congregate over the finite interval for the Cornell and screened Cornell potentials [17]. In addition, the quadrature points used in Eq. (42) lie symmetrically in the interval $(-1, 1)$ and crowd near two endpoints. Therefore, the oscillating wave function cannot be well approximated by the Legendre functions if ξ is chosen inappropriately; in that case, it leads to low accuracy. The dependence of eigenvalues on ξ will be discussed numerically in Sec. IV C.

D. Matrix equation

Employing the variable transformation [Eq. (15)] and then using Eqs. (17)–(19), (30)–(32), and (42), the subtracted integral equation [Eq. (13)] is approximated by the matrix equation

$$E\hat{\phi}(s_i) = T_i\hat{\phi}(s_i) + (K_{ii}^{1a} + K_{ii}^{1b} + K_{ii}^{2a} + K_{ii}^{2b} + K_{ii}^{2c} + K_{ii}^{2d})\hat{\phi}(s_i) + \sum_{j\neq i}(K_{ij}^{1a'} + K_{ij}^{1b'} + K_{ij}^{2a'} + K_{ij}^{2b'} + K_{ij}^{2c'} + K_{ij}^{2d'})\hat{\phi}(s_j), \tag{43}$$

where the diagonal elements are

$$T_i = \frac{p_i^2}{2\mu}, \qquad K_{ii}^{1a} = -\frac{\alpha}{\pi}p_i P_l(z'_{\beta i})\left(\frac{\pi^2}{2} - \pi\arctan\frac{\beta}{p_i}\right) + \frac{\alpha}{\pi}p_i P_l(z'_{\beta i})\sum_{j\neq i}\frac{Q_0(z_{\beta ij})}{p_j}\frac{2\xi}{(1-s_j)^2}w_j,$$

$$K_{ii}^{2a} = \frac{\lambda}{\pi p_i}P_l'(z'_{\eta i})\left(\frac{\pi^2}{2} - \pi\arctan\frac{\eta}{p_i}\right) - \frac{\lambda}{\pi p_i}P_l'(z'_{\eta i})\sum_{j\neq i}\frac{Q_0(z_{\eta ij})}{p_j}\frac{2\xi}{(1-s_j)^2}w_j,$$

$$K_{ii}^{2b} = \frac{\lambda}{\eta}(1 - P_l(z'_{\eta i})) - \frac{\lambda}{\pi p_i^2}P_l(z'_{\eta i})\sum_{j\neq i}Q_0'(z_{\eta ij})(s_i - s_j)\frac{2\xi}{(1-s_j)^2}\tilde{w}_j(s_i), \qquad K_{ii}^{1b} = \frac{\alpha}{\pi p_i}\omega_{l-1}(z'_{\beta i})p_i\frac{2\xi}{(1-s_i)^2}w_i,$$

$$K_{ii}^{2c} = -\frac{\lambda}{\pi p_i^2}\omega'_{l-1}(z'_{\eta i})\frac{2\xi}{(1-s_i)^2}w_i, \qquad K_{ii}^{2d} = \theta(\eta)\frac{\lambda}{\pi p_i^2}\frac{2\xi}{(1-s_i)^2}\tilde{w}_i(s_i)P_l(z_{\eta ii})W_i'(s_i)\lim_{\substack{t\to s\\ s\to s_i}}Q_0'(z_\eta)(s-t)^2, \tag{44}$$

and the nondiagonal elements are

$$K_{ij}^{1a'} = -\frac{\alpha}{\pi p_i} p_j P_l(z_{\beta ij}) Q_0(z_{\beta ij}) \frac{2\xi}{(1-s_j)^2} w_j, \qquad K_{ij}^{2a'} = \frac{\lambda}{\pi p_i^2} P_l'(z_{\eta ij}) Q_0(z_{\eta ij}) \frac{2\xi}{(1-s_j)^2} w_j,$$

$$K_{ij}^{2b'} = \frac{\lambda}{\pi p_i^2} P_l(z_{\eta ij}) Q_0'(z_{\eta ij})(s_i - s_j) \frac{2\xi}{(1-s_j)^2} \tilde{w}_j(s_i), \qquad K_{ij}^{1b'} = \frac{\alpha}{\pi p_i} \omega_{l-1}(z_{\beta ij}) p_j \frac{2\xi}{(1-s_j)^2} w_j,$$

$$K_{ij}^{2c'} = -\frac{\lambda}{\pi p_i^2} \omega_{l-1}'(z_{\eta ij}) \frac{2\xi}{(1-s_j)^2} w_j, \qquad K_{ij}^{2d'} = \theta(\eta) \frac{\lambda}{\pi p_i^2} \frac{2\xi}{(1-s_i)^2} \tilde{w}_i(s_i) P_l(z_{\eta ij}) W_j'(s_i) \lim_{\substack{t\to s \\ s\to s_i}} Q_0'(z_\eta)(s-t)^2. \quad (45)$$

In Eqs. (44) and (45),

$$p_i = \xi \frac{1-s_i}{1+s_i}, \qquad z_{\beta ij} = \frac{p_i^2 + p_j^2 + \beta^2}{2p_i p_j}, \qquad z_{\beta i}' = z_{\beta ii}, \qquad z_{\eta ij} = \frac{p_i^2 + p_j^2 + \eta^2}{2p_i p_j}, \qquad z_{\eta i}' = z_{\eta ii}, \quad (46)$$

and $\theta(\eta)$ is a step function defined as

$$\theta(\eta) = \begin{cases} 1, & \eta = 0, \\ 0, & \eta > 0. \end{cases} \quad (47)$$

The terms K_{ii}^{1a}, K_{ii}^{1b}, K_{ii}^{2a}, K_{ii}^{2b}, K_{ii}^{2c}, $K_{ij}^{1a'}$, $K_{ij}^{1b'}$, $K_{ij}^{2a'}$, $K_{ij}^{2b'}$, $K_{ij}^{2c'}$ in Eqs. (44) and (45) can be obtained and understood easily. K_{ii}^{2d} and $K_{ij}^{2d'}$ are from the derivative of $F_2(s,t)$ and are obtained by using Eqs. (19) and (32). The matrix equation [Eq. (43)] is free of singularity because the double-pole singularity possessed by the screened Cornell and Cornell potentials is treated completely. Just like in Eq. (13), both the screened Cornell potential and the Cornell potential in Eq. (43) are tackled in the same manner.

IV. NUMERICAL RESULTS AND DISCUSSIONS

In this paper, the Schrödinger equation is solved numerically with screened linear, linear, screened Cornell [17], and Cornell potentials. Four numerical methods are applied: In Method I, we discretize straightforwardly all integrals in the unsubtracted integral equation [Eq. (10)] with the logarithmic singularity and the double-pole singularity by using the Gauss-Legendre quadrature rule, then solve the obtained matrix equation. In Method II, we apply the Gauss-Legendre quadrature rule to all integrals in the subtracted integral equation [Eq. (13)], which is obtained from Eq. (10) by employing the Landé subtraction method, and then solve the resulting matrix equation with the left principal-value singularity. Method III is a combination method in which the Landé subtraction method is applied to remove the logarithmic singularity and to weaken the double-pole singularity, and then the left principal-value singularity is absorbed into quadrature weights by employing the spectral method, and finally, the integral equation is transformed into a singularity-free matrix equation [Eq. (43)]. The former two methods belong to the Nyström method, and Method III is a spectral method. The numerical results calculated by the three methods are compared with each other and with the results for the Schrödinger equation represented in configuration space (CS) by implementing the Numerov method (the fourth method).

A. Screened linear potential

The eigenvalues for the screened linear potential are calculated by four different methods and then compared with each other in Table I.

As pointed out in Refs. [17,27,47], the screened linear potential has singularities as well as the linear potential. The singularities will become stronger when the screening factor η decreases and will be weakened as η increases. As shown in Table I and discussed in Refs. [17,47], Method I will not be appropriate for a small screening factor or for linear potential. But it can give correct results when η is large enough. Method II gives good results for large η, and the error will increase as η decreases. Method III works well in both small and large screening factor cases. We note that the eigenvalues calculated by Method I and Method II are smaller than the eigenvalues obtained in configuration space which are expected to be good. Because the screened linear potential is singular, the eigenvalues will be underestimated for Methods I and II.

TABLE I. Comparison between the eigenvalues for the screened linear potential obtained by different methods. The symbol $\times$ means the calculated results are wrong. $\mu = 1$ GeV, $\alpha = 0$, $\lambda = 1$ GeV^2, $L = 0$, $N = 30$, and $\xi = 1$ GeV. The eigenvalues and η are in GeV. n_r is equal to the number of nodes in the radial wave function.

η	n_r	Method I	Method II	Method III	CS
0.01	0	$\times$	1.77	1.85	1.85
	1	$\times$	3.04	3.24	3.22
	2	$\times$	3.99	4.38	4.33
0.1	0	1.28	1.74	1.81	1.76
	1	2.44	2.92	3.06	2.97
	2	3.54	3.78	4.05	3.88
0.5	0	1.41	1.41	1.41	1.41
	1	1.91	1.91	1.91	1.91
	2	2.00	2.00	2.00	2.00

TABLE II. The eigenvalues for the linear potential ($\eta = 0$) obtained by solving Eq. (43). $\mu = 1$ GeV, $\alpha = 0$, $\lambda = 1$ GeV^2, $N = 80$, $\xi = 1$ GeV. The eigenvalues and η are in GeV. n_r is equal to the number of nodes in the radial wave function, and L is the orbital angular momentum.

	Method III			Ref. [57]		
n_r	$L = 0$	$L = 1$	$L = 2$	$L = 0$	$L = 1$	$L = 2$
0	1.855757	2.667838	3.371806	1.855757	2.667829	3.371784
1	3.244608	3.876822	4.468399	3.244607	3.876792	4.468302
2	4.381671	4.927055	5.452036	4.381671	4.926994	5.451836
3	5.386614	5.877982	6.357636	5.386614	5.877880	6.357305

On the contrary, as discussed in Secs. III C and IV D, when the double-pole singularity is handled completely, the obtained eigenvalues by Method III will be larger than the true values.

B. Other potentials

By employing Method III, the eigenvalues for the linear, screened Cornell, and Cornell potentials are calculated; see Tables II, III, and IV, respectively. The obtained results are very good and are in agreement with the results in Ref. [46] and the results calculated in configuration space (CS).

C. Effects of the parameter ξ

As an example to show numerically the dependence of the calculated eigenvalues on the mapping parameter ξ, we employ Method III to solve the subtracted integral equation [Eq. (13)]—i.e., we need to solve the matrix equation [Eq. (43)]. The eigenvalues for the ground state are shown in Fig. 1. The dotted line is for $N = 20$, and the dashed line is for $N = 40$. The dot-dashed line is for the eigenvalue obtained by implementing the Numerov method in configuration space (CS), which is independent of ξ.

The dependence of eigenvalues on ξ is not simple. As shown in the upper panel in Fig. 1, when N is small, the calculated eigenvalues oscillate with ξ, as ξ is very small or very large, and there are many relative minimums; see the dotted line. Therefore, the minimum is not unique as

TABLE III. The eigenvalues for the screened Cornell potential. $\alpha = 0.50667$, $\beta = 0$ GeV, $\mu = 0.685$ GeV, $\lambda = 0.1694$ GeV^2, $\xi = 1$ GeV, $N = 120$. The eigenvalues and η are in GeV. n_r is equal to the number of nodes in the radial wave function, and L is the orbital angular momentum.

		Method III			CS		
η	n_r	$L = 0$	$L = 1$	$L = 2$	$L = 0$	$L = 1$	$L = 2$
	0	3.0449	3.3950	3.6139	3.0448	3.3949	3.6138
0.1	1	3.5131	3.7097	3.8579	3.5129	3.7095	3.8577
	2	3.7951	3.9293	4.0365	3.7948	3.9290	4.0362
	0	3.0054	3.2961	3.4469	3.0054	3.2961	3.4469
0.2	1	3.3641	3.4821	3.5486	3.3641	3.4821	3.5486
	2	3.5118	3.5584	3.5775	3.5118	3.5584	3.5775

TABLE IV. Same as Table III, except for $\eta = 0$ (Cornell potential) and $N = 80$.

	Method III			Ref. [46]		
n_r	$L = 0$	$L = 1$	$L = 2$	$L = 0$	$L = 1$	$L = 2$
0	3.0869	3.4988	3.7868	3.0869	3.4988	3.7868
1	3.6748	3.9544	4.1868	3.6748	3.9544	4.1868
2	4.1093	4.3388	4.5407	4.1094	4.3388	4.5407

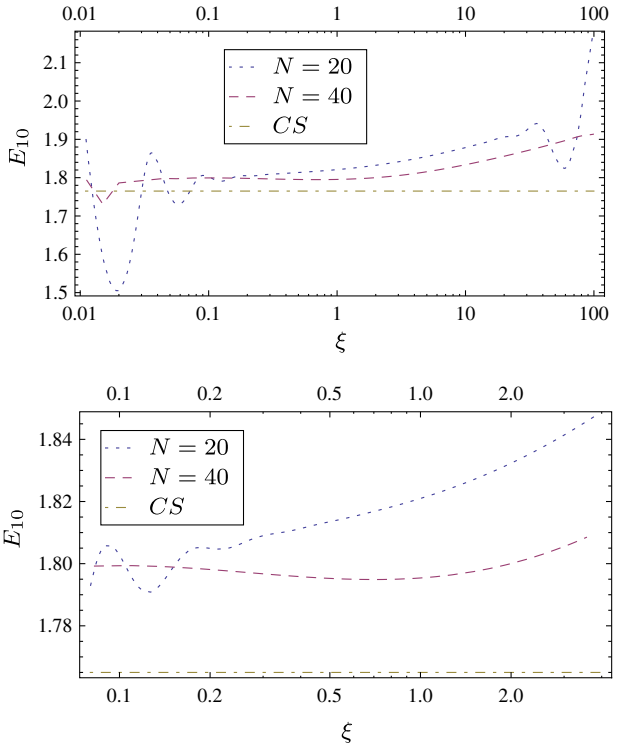

FIG. 1 (color online). The dependence of the ground-state eigenvalue (in GeV) on the parameter ξ (in GeV). The eigenvalues for the screened linear potential are calculated in momentum space by employing Method III for $N = 20$ (the dotted line) and for $N = 40$ (the dashed line), and in configuration space (CS) (the dot-dashed line) by the Numerov method. $\eta = 0.1$ GeV, $\mu = 1$ GeV, $\lambda = 1$ GeV^2, $\alpha = 0$.

described in Eq. (39), and again is not a good approximation of the actual eigenvalues.

With the increase of N, the eigenvalues obtained become better, and the dependence of eigenvalues on ξ becomes weaker; see the dashed line in the upper panel in Fig. 1. As we investigate in detail the behavior of eigenvalues on ξ in the small interval (0.1, 2), we find that the dashed line has fine structure; see the lower panel in Fig. 1, in which the line looks straight in the interval (0.1, 2) in the upper panel. We note that the structure of the dashed line for $N = 40$ becomes simpler than the structure of the dotted line for $N = 20$. It is expected that the dependence of the calculated eigenvalues on ξ can be neglected when N is large enough.

From Fig. 1, we can find that the eigenvalues calculated for $0.1 < \xi < 10$ are good. Based on discussions in Sec. III C and the calculated results, we assume that—in particular, for small N—the calculated eigenvalues will be unreliable in practice when ξ is far from the typical momentum $(\mu\lambda)^{1/3}$ and will be reliable when ξ is close to the typical momentum. The discussions for the ground state are also expected to be valid for the excited states. Therefore, we take $\xi = 1$ GeV when calculating the eigenvalues in this paper.

D. Convergence directions of the calculated eigenvalues

From Table I, we find that the eigenvalues calculated by using Methods I and II are smaller than the eigenvalues obtained in configuration space which are expected to be good, while the eigenvalues calculated by Method III are greater than the eigenvalues obtained in configuration space. This observation coincides with the conclusion drawn in the Appendix—i.e., the convergence directions of the eigenvalues yielded by Methods I and II are abnormal, while that of the eigenvalues yielded by Method III is normal. That the convergence direction is normal or abnormal results from whether the kernels are singularity free or singular, and/or from whether the chosen numerical method is appropriate or inappropriate. In the example shown in Table I, the eigenvalues calculated by Methods I and II are smaller than the eigenvalues calculated by the Numerov method. That is because the kernels are singular for Methods I and II.

As shown in the Appendix, we suggest that abnormal convergence directions of the calculated eigenvalues can be regarded as a clue of the possible unreliability of the calculated results. When the obtained eigenvalues converge abnormally, we should give a more careful check of the integral equation and the chosen numerical method than ever.

E. Accuracy and singularity

The accuracy of the yielded results depends not only on the numerical methods but also on the singularities [17,27,47] in kernels. As shown in Table I, the results obtained by Method III are better than those from Method II, and the results calculated by Method II are better than those from Method I, because the singularities are handled completely for Method III, while the singularity is a Cauchy principal-value singularity for Method II and is of second order for Method I.

In Refs. [17,47], it was pointed out that the singularity will be weakened, and then the accuracy of the calculated eigenvalues will increase as the screening parameters become larger. This viewpoint is testified to again by the numerical results; see Table I. The results in Table I also show that the method in which the screening parameters β, η are introduced as factors to regulate the singularities is inappropriate if high accuracy is needed.

V. CONCLUSIONS

In this paper, we solve numerically the Schrödinger equation in momentum space with the screened linear, linear, screened Cornell and Cornell potentials by employing a combined method (the Landé subtraction method plus the spectral method). We adopt the Landé subtraction method to eliminate the logarithmic singularity and weaken the double-pole singularity possessed by the momentum-space potentials. The left Cauchy principal-value singularity is absorbed into the quadrature weights by applying the spectral method with the Gauss-Legendre quadrature rule. The results can be yielded with very high accuracy because singularities, especially the double-pole singularity, are handled completely.

In this paper, we note that the eigenvalues calculated by numerical methods have definite convergence directions. Generally speaking, an abnormal convergence direction implies that the yielded results may be unreliable and there is a possible problem in the numerical method or in the integral equation. The abnormal convergence direction gives us a warning, and we should be more cautious than ever to determine whether the results are reliable or not.

Moreover, we discuss the dependence of the calculated eigenvalues on the mapping parameter ξ. The dependence is not as simple as expected before and has somewhat complex structure, especially for small N. When N is small, ξ cannot be far from the typical momentum to obtain good results. The dependence will decrease and become simple as N increases, and it will become very weak when N is large enough.

APPENDIX A: CONVERGENCE DIRECTIONS OF THE NUMERICAL EIGENVALUES

1. Normal convergence directions of the numerical eigenvalues

a. Formulas

Applying the analytical results [Eq. (39)] obtained in Sec. III C to numerical methods leads to the convergence

directions of the calculated eigenvalues. The expansion method case has already been discussed in Refs. [38,39]. For completeness, we list the results firstly.

Approximating the eigenfunctions in the form

$$\psi(p) \approx \psi^N(p) = \sum_{i=1}^{N} a_i h_i(p), \tag{A1}$$

we can have the matrix equation from Eq. (33),

$$E^N M\mathbf{a} = L\mathbf{a}, \qquad F(\psi^N) = E^N \equiv \frac{\mathbf{a}^{\mathbf{T}} L\mathbf{a}}{\mathbf{a}^{\mathbf{T}} M\mathbf{a}}, \tag{A2}$$

where $\mathbf{a} = \{a_1, \ldots, a_N\}$, and

$$\begin{aligned} L_{ij} &= \int h_i^\dagger(p) K(p, p') h_j(p') p^2 p'^2 dp dp', \\ M_{ij} &= \int h_i^\dagger(p) h_j(p) p^2 dp. \end{aligned} \tag{A3}$$

In the case of the orthonormal set $\{h_i\}$, M becomes the identity. Employing Eqs. (35), (37), and (39), the following can be obtained for the matrix equation [Eq. (A2)]:

$$\begin{aligned} &E_{\min} \le E^N_{\min} \le E^N_1 \le \cdots \le E^N_i \cdots \le E^N_{\max} \le E_{\max}, \\ &E_{\min} \le E^{N+1}_{\min} \le E^N_{\min}, \ldots, E^N_{\max} \le E^{N+1}_{\max} \le E_{\max}, \end{aligned} \tag{A4}$$

which is somewhat different from the results given in Ref. [38]. The results in Eq. (A4) are obvious. The calculated eigenvalues will be good approximations of the actual ones if the numerical method is reliable; therefore, we have the first line in Eq. (A4). When more points or more basis functions are used in numerical calculations, the obtained results should be more accurate and thus closer to the actual ones; therefore, we have the second line in Eq. (A4).

Now we consider the Nyström method case. From Eqs. (33) and (35), we have

$$F(\psi^N) = \frac{(\psi^N, K\psi^N)}{(\psi^N, \psi^N)} = \frac{\sum_{i,j=1}^N c_i c_j \psi_i^N K_{ij} \psi_j^N}{\sum_{i=1}^N c_i \psi_i^N \psi_i^N}, \tag{A5}$$

where $\psi_i^N = \psi^N(p_i)$, $K_{ij} = K(p_i, p_j)$, and c_i is the weight for the chosen quadrature rule multiplied by p_i^2. Setting

$$\frac{\partial F}{\partial \psi_m^N} = 0, \qquad m = 1, 2, \ldots, N, \tag{A6}$$

we can obtain

$$\frac{\psi_m^N(\sum_{i,j=1}^N c_i c_j \psi_i^N K_{ij} \psi_j^N) - (\sum_{i=1}^N c_i \psi_i^N K_{mi})(\sum_{i=1}^N c_i \psi_i^N \psi_i^N)}{(\sum_{i=1}^N c_i \psi_i^N \psi_i^N)^2} = 0 \tag{A7}$$

if the matrix K_{ij} is symmetric; that is,

$$\begin{aligned} E^N \psi_m^N &= \sum_{i=1}^N c_i K_{mi} \psi_i^N, \\ E^N &= \frac{\sum_{i,j=1}^N c_i c_j \psi_i^N K_{ij} \psi_j^N}{\sum_{i=1}^N c_i \psi_i^N \psi_i^N} = F(\psi^N). \end{aligned} \tag{A8}$$

The above equation is just the matrix equation yielded by discretizing the integral equation [Eq. (33)]. Therefore, the matrix equation [Eq. (A8)] is the eigenvalue equation to obtain the eigenvalues and eigenfunctions for the integral equation [Eq. (33)]. Equation (A8) shows explicitly that the obtained eigenvalue E^N is indeed a stationary point of the functional $F(\psi^N)$, and the functional is stationary at ψ_i^N, $i = 1, \ldots, N$, where ψ^N is the corresponding eigenfunction. Therefore, the properties [Eq. (A4)] of the calculated eigenvalues for the expansion method will hold for the Nyström method.

For the spectral method case, Eq. (A5) becomes

$$F(\psi^N) = \frac{(\psi^N, K\psi^N)}{(\psi^N, \psi^N)} = \frac{\sum_{i,j=1}^N c_i c_j \psi_i^N \tilde{K}_{ij} \psi_j^N}{\sum_{i=1}^N c_i \psi_i^N \psi_i^N}, \tag{A9}$$

where $\tilde{K}_{ij}$ is not $K(p_i, p_j)$ again, but rather is constructed by the chosen spectral method. c_i is not a simple quadrature weight again but a factor, $w_i p_i^2 2\xi/(1 - s_i)^2$ in this paper. If $\tilde{K}_{ij}$ is symmetric on the indices i and j, the conclusions in Eq. (A4) will hold for the spectral method, too. $\tilde{K}_{ij}$ is symmetric in the case of the screened linear potential and the screened Cornell potential; therefore, the convergence directions of the eigenvalues for these two potentials will be normal when the singularities are handled completely and will be abnormal when kernels are singular; see Tables I and III. $\tilde{K}_{ij}$ is not a symmetric matrix for the spectral method applied in this paper in the case of the linear potential or the Cornell potential; however, it is surprising that the calculated eigenvalues for these two potentials converge normally when the singularities are handled completely; see Table II.

b. Discussions

The properties [Eq. (A4)] of the numerical eigenvalues are of great practical importance. Equation (A4) implies that the convergence of each eigenvalue is monotonic in N, and this is certainly useful numerically. We call the convergence direction of a numerical eigenvalue obeying Eq. (A4) a *normal convergence direction*; otherwise, it is an *abnormal convergence direction*.

If the calculated eigenvalues obey the normal convergence directions, the results will be expected to be reliable. If one obtained eigenvalue converges abnormally, however,

it is quite likely that there is a problem in the result. The problem may arise from the adopted numerical method or from the bad behavior of the eigenvalue equation to be solved. This is valid not only for an eigenvalue equation represented in momentum space but also for one represented in configuration space.

According to Eq. (A4), the convergence directions are obvious and clear for the small eigenvalues close to the ground-state eigenvalue $E_{\min}$, which converge from the right side to the corresponding actual values. They are also obvious and clear for the large eigenvalues close to the greatest eigenvalue $E_{\max}$, that converge from the left side to exact values. However, the convergence directions of the eigenvalues lying between the smallest and the greatest eigenvalues will be ambiguous—that is to say, it is not definite whether the numerical eigenvalues in the middle converge to the exact values from the left side or from the right side.

c. Examples

In this subsection, we illustrate the conclusion that the reliable numerical eigenvalues will have normal convergence directions by using some examples.

As shown in Tables V and VI, both the eigenvalues for the spinless Salpeter equation with the Coulomb potential calculated by employing the expansion method in momentum space and the eigenvalues for the Schrödinger equation with the screened Coulomb potential in momentum space solved using the Nyström method are reliable, and their convergence directions are normal. The conclusion of Eq. (A4) is appropriate not only for momentum space problems but also for configuration space problems; see Tables VII, VIII, and IX.

2. Abnormal convergence directions of the numerical eigenvalues

Generally speaking, the calculated eigenvalues will be reliable if their convergence directions are normal, while an abnormal convergence direction implies a possible unreliability. As shown in Tables I and X, when the kernels are singular [27] (i.e., when η and b are small), the obtained eigenvalues have abnormal convergence directions, while when the kernels are free of singularities (i.e., when η and b are large) the convergence directions of the calculated eigenvalues become normal.

In the case of the screened Coulomb potential or the screened linear potential, abnormal convergence directions arise from the bad behavior of kernels. Sometimes, the problem stems from the chosen numerical method; see Table XI. The convergence direction oscillates as N increases. In this example, the largest eigenvalue approaches the exact one from two sides. This bad behavior [38] means that there is a threshold value N_0, in the sense that when N exceeds N_0, the effects of ill conditioning seriously impair the accuracy. This ill conditioning comes from the use of special basis functions.

Sometimes, although the convergence directions are abnormal, the results are still good; see the numerical results listed in Refs. [47,31,46]. In summary, an abnormal convergence direction serves only as a sign that the

TABLE V. The eigenvalues for the spinless Salpeter equation with the Coulomb potential are calculated by employing the expansion method in momentum space (MS) and are compared with the eigenvalues obtained in configuration space (CS). The data are from Table I in Ref. [26].

n	1	2	3	4	10
MS	−13.606595	−3.4015706	−1.5117909	−0.8503765	−0.1360585
CS	−13.606604	−3.4015717	−1.5117912	−0.8503766	−0.1360584

TABLE VI. The eigenvalues for the Schrödinger equation with the screened Coulomb potential in momentum space are calculated by using the Nyström method. b is the screening parameter. The data are from Table IV in Ref. [17].

x_N	n	$b = 0$	$b = 10^{-6}$	$b = 10^{-3}$	$b = 10^{-1}$
	1	−0.499800	−0.499799	−0.498801	−0.406861
20	2	−0.124978	−0.124977	−0.123981	−0.0499079
	3	−0.0555583	−0.0555573	−0.0545646	−0.00320554
	1	−0.499940	−0.499939	−0.498941	−0.406999
30	2	−0.124995	−0.124994	−0.123998	−0.0499224
	3	−0.0555635	−0.0555625	−0.0545698	−0.00320746
	1	−0.5			
Exact	2	−0.125			
	3	−0.0555556			

TABLE VII. The eigenvalues for the Schrödinger equation with the Hulthén potential in configuration space are produced by employing the expansion method. The data are from Table I in Ref. [58].

N	5	10	Exact
Energy	0.016805	0.016805555555	0.1680555...

TABLE VIII. The eigenvalues for the spinless Salpeter equation with the funnel potential (Cornell potential) represented in configuration space. $V(|\mathbf{x}|) = -\kappa/|\mathbf{x}| + a|\mathbf{x}|$. $\mu = m = 1$ GeV, $\beta = 1$, $\kappa = 0.456$, $a = 0.211$ GeV^2, and the size $d \times d$ of the energy matrix (H_{ij}). All eigenvalues are given in units of GeV. The data are from Table 4 in Ref. [59].

State	1×1	2×2	20×20
1S	2.5767	2.5182	2.5162
2S		3.4499	3.1570

calculated results may be unreliable. When the calculated eigenvalues converge abnormally, we should be cautious and then make a more careful examination of the integral equation and the numerical method to determine whether the results are indeed reliable or not.

3. Convergence direction and furcation

Both abnormal convergence direction and furcation [17,47,48] can be used as indicators of the unreliability of the obtained results and/or the bad behavior of the integral equation. Both of them are related to singularities in potentials. Abnormal convergence direction is about eigenvalues, while furcation phenomenon emerges in the obtained eigenfunctions.

Abnormal convergence directions of the calculated eigenvalues arise from singularities in kernels and/or inappropriate numerical methods. When abnormal convergence direction occurs, we should be cautious of whether the results are reliable or not (see the previous subsection), and then carefully check the integral equation and the applied numerical method.

TABLE IX. The eigenvalues of the semirelativistic Hamiltonian $H = 2\sqrt{\mathbf{p}^2 + m^2} + V(r)$ with a harmonic oscillator potential $V(r) = ar^2$ are calculated by the expansion method. The data are from Table 1 in Ref. [60].

	$l = 0$				$l = 1$			
	1S	2S	3S	4S	1P	2P	3P	4P
1	4.14531				5.12166			
3	3.91571	7.08622	11.94458		5.03946	7.68220	14.80138	
10	3.82522	5.80930	7.76609	9.90246	4.89944	6.72710	8.54739	11.20168
25	3.82494	5.79112	7.48323	9.01617	4.90149	6.69298	8.28585	9.74304
Exact	3.82493	5.79102	7.48208	9.00749	4.90145	6.69305	8.28464	9.74276

TABLE X. The eigenvalues for the singularity-free Schrödinger equation (C) and the singular Schrödinger equation (NC) with the screened Coulomb potential are calculated by employing the Nyström method with the extended Simpson's rule (SR) and with the extended trapezoidal rule (TR). b is the screening parameter. The data are from Table III in Ref. [17].

b	n	TR(C)	TR(NC)	SR(C)	SR(NC)
	1	−0.397332	−0.397331	−0.397332	−0.397331
10^{-1}	2	−0.0488747	−0.0488742	−0.0488746	−0.0488742
	3	−0.00306981	−0.00306958	−0.00306981	−0.00306958
	1	−0.489129	−0.491555	−0.489129	−0.492217
10^{-3}	2	−0.122730	−0.125155	−0.122731	−0.125835
	3	−0.0541873	−0.0566106	−0.0541916	−0.0573194
	1	−0.490127	−0.513594	−0.490127	−0.51679
10^{-6}	2	−0.123726	−0.147192	−0.123727	−0.150749
	3	−0.0551799	−0.0786442	−0.0551842	−0.0827475

TABLE XI. The largest eigenvalue for the equation $\gamma x(s) = \int_0^1 (st - s^3t^3/6)x(t)dt$ calculated by an expansion method. The data are from Table 7.4.1 in Ref. [38].

N	2	4	8	Exact
Energy	0.31344	0.31357	0.31359	0.31357

The furcation phenomenon emerging in the yielded eigenfunctions results not only from singularities in potentials but also from special numerical methods which have unequal repeated weights. When furcation emerges, it is very possible that the numerical results, including eigenvalues and eigenfunctions, are of low accuracy or even bad. Furcation is due primarily to singularities in kernels. Although playing an important role in arousing the furcation phenomenon, the special numerical methods are not inappropriate but get an advantage over other methods which do not arouse furcation. One simple and typical example is that the Schrödinger equation with the screened Coulomb potential is solved by employing the Nyström method with the extended Simpson's rule [17,47].

[1] N. Brambilla *et al.* (Quarkonium Working Group), arXiv:hep-ph/0412158.
[2] S. Eidelman, B. K. Heltsley, J. J. Hernandez-Rey, S. Navas, and C. Patrignani, arXiv:1205.4189.
[3] G. S. Bali, Phys. Rep. **343**, 1 (2001).
[4] N. Brambilla, S. Eidelman, B. K. Heltsley, R. Vogt, G. T. Bodwin, E. Eichten, A. D. Frawley, A. B. Meyer *et al.*, Eur. Phys. J. C **71**, 1534 (2011).
[5] D. M. Asner, T. Barnes, J. M. Bian, I. I. Bigi, N. Brambilla, I. R. Boyko, V. Bytev, K. T. Chao *et al.*, Int. J. Mod. Phys. A **24**, 499 (2009).
[6] E. Eichten, K. Gottfried, T. Kinoshita, J. B. Kogut, K. D. Lane, and T.-M. Yan, Phys. Rev. Lett. **34**, 369 (1975); **36**, 1276(E) (1976).
[7] E. Eichten, K. Gottfried, T. Kinoshita, K. D. Lane, and T.-M. Yan, Phys. Rev. D **17**, 3090 (1978); **21**, 313(E) (1980).
[8] D. P. Stanley and D. Robson, Phys. Rev. D **21**, 3180 (1980).
[9] S. Godfrey and N. Isgur, Phys. Rev. D **32**, 189 (1985).
[10] W. Lucha, F. F. Schoberl, and D. Gromes, Phys. Rep. **200**, 127 (1991).
[11] C. Semay and B. Silvestre-Brac, Nucl. Phys. **A618**, 455 (1997).
[12] S. N. Gupta, J. M. Johnson, W. W. Repko, and C. J. Suchyta, III, Phys. Rev. D **49**, 1551 (1994).
[13] T. Barnes, S. Godfrey, and E. S. Swanson, Phys. Rev. D **72**, 054026 (2005).
[14] E. Laermann, F. Langhammer, I. Schmitt, and P. M. Zerwas, Phys. Lett. B **173**, 437 (1986).
[15] K. D. Born, E. Laermann, N. Pirch, T. F. Walsh, and P. M. Zerwas, Phys. Rev. D **40**, 1653 (1989).
[16] G. S. Bali, H. Neff, T. Düssel, T. Lippert, and K. Schilling (SESAM Collaboration), Phys. Rev. D **71**, 114513 (2005).
[17] J.-K. Chen, Phys. Rev. D **86**, 036013 (2012); Erratum (to be published).
[18] P. Gonzalez, A. Valcarce, H. Garcilazo, and J. Vijande, Phys. Rev. D **68**, 034007 (2003).
[19] J. Vijande, P. Gonzalez, H. Garcilazo, and A. Valcarce, Phys. Rev. D **69**, 074019 (2004).
[20] J. Segovia, A. M. Yasser, D. R. Entem, and F. Fernandez, Phys. Rev. D **78**, 114033 (2008).
[21] J. Vijande, G. Krein, and A. Valcarce, Eur. Phys. J. A **40**, 89 (2009).
[22] E. H. Mezoir and P. Gonzalez, Phys. Rev. Lett. **101**, 232001 (2008).
[23] J. Segovia, D. R. Entem, and F. Fernandez, Phys. Lett. B **662**, 33 (2008).
[24] B.-Q. Li, C. Meng, and K.-T. Chao, Phys. Rev. D **80**, 014012 (2009).
[25] F. Karsch, M. T. Mehr, and H. Satz, Z. Phys. C **37**, 617 (1988).
[26] J. W. Norbury, K. M. Maung, and D. E. Kahana, Phys. Rev. A **50**, 3609 (1994).
[27] Analytically speaking, there will be no singularity in the momentum-space screened linear potential or the screened Cornell potential if the screening parameters are greater than zero. Numerically speaking, however, these potentials behave badly and the obtained numerical results become unreliable when the screening parameters become small. These screened potentials need the same treatment as the Cornell potential and the linear potential. In this paper, we shall use the term *singularity* rather widely to refer to the bad behaviors of the potentials. More details can be found in Refs. [17,47].
[28] T. W. Chiu, J. Phys. A **19**, 2537 (1986).
[29] D. Eyre and J. P. Vary, Phys. Rev. D **34**, 3467 (1986).
[30] J. R. Spence and J. P. Vary, Phys. Rev. D **35**, 2191 (1987).
[31] J. W. Norbury, K. M. Maung, and D. E. Kahana, Phys. Rev. A **50**, 2075 (1994).
[32] K. M. Maung, D. E. Kahana, and J. W. Norbury, Phys. Rev. D **47**, 1182 (1993).
[33] W. Lucha, H. Rupprecht, and F. F. Schoberl, Phys. Rev. D **45**, 1233 (1992).
[34] L. P. Fulcher, Z. Chen, and K. C. Yeong, Phys. Rev. D **47**, 4122 (1993).
[35] L. J. Nickisch, L. Durand, and B. Durand, Phys. Rev. D **30**, 660 (1984); **30**, 1995(E) (1984).
[36] H. C. Jean, D. Robson, and A. G. Williams, Phys. Rev. D **50**, 5873 (1994).
[37] A. Tang and J. W. Norbury, Phys. Rev. E **63**, 066703 (2001).

[38] L. M. Delves and J. L. Mohamed, *Computational Methods for Integral Equations* (Cambridge Univeristy Press, New York, 1992).
[39] C. T. H. Baker, *The Numerical Treatment of Integral Equations* (Oxford University Press, New York, 1977).
[40] R. S. Anderssen, F. R. de Hoog, and M. A. Lukas, *The Application and Numerical Solution of Integral Equations* (Sijthoff & Noordhoff, Netherlands, 1980); K. E. Atkinson, *The Numerical Solution of Integral Equations of the Second Kind* (Cambridge University Press, New York, 1997).
[41] W. H. Press, S. A. Teukolsky, W. T. Vetterling, and B. P. Flannery, *Numerical Recipes in C: The Art of Scientific Computing* (Cambridge University Press, New York, 1992).
[42] Y. R. Kwon and F. Tabakin, Phys. Rev. C **18**, 932 (1978).
[43] R. H. Landau, Phys. Rev. C **27**, 2191 (1983).
[44] R. H. Landau, *Quantum Mechanics II: A Second Course in Quantum Theory* (Wiley, New York, 1990).
[45] J. H. Sloan, J. Comput. Phys. **3**, 332 (1968).
[46] A. Deloff, Ann. Phys. (Amsterdam) **322**, 2315 (2007).
[47] J. K. Chen, Few-Body Syst. **54**, 2081 (2013).
[48] When the singular integral equation is solved by employing the quadrature method with repeated unequal weights, the calculated eigenfunctions will divide into branches. To distinguish it from the bifurcation in the nonlinear problem, we call this peculiar phenomenon *furcation*; see Refs. [17,47].
[49] H. R. Kutt, Numer. Math. **24**, 205 (1975).
[50] P. Linz, Computing **35**, 345 (1985).
[51] A. Tang, arXiv:hep-ph/0103035.
[52] M. Abramowitz and I. Stegun, *Handbook of Mathematical Functions* (Dover, New York, 1972).
[53] F. W. J. Olver, D. W. Lozier, R. F. Boisvert, and C. W. Clark, *NIST Handbook of Mathematical Functions* (Cambridge Univerisity Press, New York, 2010).
[54] M. Carley, SIAM J. Sci. Comput. **29**, 1207 (2007).
[55] P. Kolm and V. Rokhlin, Report No. YALEU/DCS/RR-1190, 2000.
[56] R. Courant and D. Hilbert, *Methods of Mathematical Physics I* (Interscience, New York, 1966).
[57] The data presented in Table II are the eigenvalues in Ref. [46] multiplied by $\lambda^{1/3}(2\mu)^{-1/3}$.
[58] C. Stubbins, Phys. Rev. A **48**, 220 (1993).
[59] W. Lucha and F. F. Schoberl, Phys. Rev. A **56**, 139 (1997).
[60] W. Lucha and F. F. Schöberl, Int. J. Mod. Phys. C **11**, 485 (2000).